# A Ratiometric Readout Circuit for Thermal-Conductivity-Based Resistive $CO_2$ Sensors

Cai, Z.; van Veldhoven, Robert H.M.; Falepin, A.; Suy, H.; Sterckx, E.; Bitterlich, C.; Makinwa, K.A.A.; Pertijs, M.A.P.

**DOI**
10.1109/JSSC.2016.2587861

**Publication date**
2016

**Document Version**
Accepted author manuscript

**Published in**
IEEE Journal of Solid State Circuits

# A Ratiometric Readout Circuit for Thermal-Conductivity-Based Resistive $CO_2$ Sensors

Zeyu Cai[1], Robert H.M. van Veldhoven[2], Annelies Falepin[3], Hilco Suy[4], Eric Sterckx[3], Christian Bitterlich[5], Kofi A.A. Makinwa[1] and Michiel A.P. Pertijs[1]

[1]Electronic Instrumentation Laboratory, Delft University of Technology, Delft, the Netherlands

[2]NXP Semiconductors, Eindhoven, the Netherlands

[3]NXP Semiconductors, Leuven, Belgium

[4] ams, BL Environmental Sensors, Eindhoven, the Netherlands

[5] ams, BL Environmental Sensors, Reutlingen, Germany

Abstract: This paper reports a readout circuit for a resistive $CO_2$ sensor, which operates by measuring the $CO_2$-dependent thermal conductivity of air. A suspended hot-wire transducer, which acts both as a resistive heater and temperature sensor, exhibits a $CO_2$-dependent heat loss to the surrounding air, allowing $CO_2$ concentration to be derived from its temperature rise and power dissipation. The circuit employs a dual-mode incremental delta-sigma ADC to digitize these parameters relative to those of an identical, but isolated, reference transducer. This ratiometric approach results in a measurement that does not require precision voltage or power references. The readout circuit uses dynamically-swapped transducer pairs to cancel their baseline-resistance, so as to relax the required dynamic range of the ADC. In addition, dynamic element matching (DEM) is used to bias the transducer pairs at an accurate current ratio, making the measurement insensitive to the precise value of the bias current. The readout circuit has been implemented in a standard 0.16 μm CMOS technology. With commercial resistive micro-heaters, a $CO_2$ sensing resolution of about 200 ppm (1σ) was achieved in a measurement time of 30 s.

Similar results were obtained with CMOS-compatible tungsten-wire transducers, paving the way for fully-integrated $CO_2$ sensors for air-quality monitoring.

Key words: $CO_2$ sensor; gas sensor; thermal conductivity; thermal resistance; resistive sensor; RDC; ratiometric; delta sigma modulator;

## I. INTRODUCTION

Carbon dioxide ($CO_2$) sensors account for a substantial share of the total gas-sensor market [1]. One reason for this is that $CO_2$ concentration is not only a measure of indoor air-quality, but is also correlated with human productivity [2], making $CO_2$ sensing an essential element in future home and building automation (HABA) systems.

For indoor $CO_2$ sensing, concentrations of up to 2500 ppm need to be measured with a resolution of better than 200 ppm [2, 3]. Moreover, the sensors need to be stable to avoid maintenance or replacement costs. Currently-available sensors that meet these requirements are based on non-dispersive infrared absorption (NDIR) or on solid-state electrolytes [4, 5]. In contrast with integrated environmental sensors, e.g. for the measurement of temperature and relative humidity [6，7，8], these $CO_2$ sensors are relatively bulky and expensive. Moreover, their power consumption, e.g. 220 mW for a typical NDIR-based $CO_2$ sensor [9], far exceeds what is needed in next-generation wireless sensor nodes for HABA systems [10].

Gas sensors based on thermal-conductivity (TC) measurement rely on the fact that the heat loss of a suspended heated wire depends on the composition of the surrounding gas. Changes in gas

composition can therefore be detected via changes in the wire's temperature. This principle forms the basis of low-cost sensors for the detection of gases such as Hydrogen, Helium, and $CO_2$, as the required heaters and sensors can be realized in IC technology [11, 12, 13]. Sensors based on TC measurement are inherently nonselective, but in typical indoor scenarios, besides the fluctuations in temperature, humidity and pressure, air composition is only altered by exhalation, which causes a noticeable change in $CO_2$ concentration. Cross-sensitivities to temperature, humidity, or pressure can be compensated by integrating auxiliary environmental sensors with the $CO_2$ sensor. However, to realize TC-based $CO_2$ sensors for monitoring indoor $CO_2$ levels is very challenging, as extremely small changes in thermal conductivity need to be measured. Based on the thermal conductivities of air and $CO_2$ at 25ºC (26 mW/K·m and 16.4 mW/K·m, respectively), a 200 ppm change in $CO_2$ concentration only leads to <80 ppm change in thermal conductivity, thus requiring a high-resolution temperature measurement, and, more critically, an extremely stable power reference (any changes in heater power will lead to errors in the measured temperature and thus errors in the measured thermal conductivity). As will be detailed in Section II, for our $CO_2$ sensor, a 50 ppm change of power corresponds to a 200 ppm error in $CO_2$ concentration. Unfortunately, the stability of on-chip power references is typically not better than 4000 ppm [14，15，16], which is equivalent to 1.6% error in $CO_2$ concentration for our sensor. Prior TC-based $CO_2$ sensors employ expensive off-chip circuits to control the heating power [12, 13]. In addition, such sensors typically employ micro-machined structures with separate transducers for heating and temperature sensing [17, 18], requiring relatively complex and costly processing steps. Using a suspended resistor as both a heating and sensing element significantly simplifies the fabrication process [19], but it requires a readout circuit that is capable of accurately measuring both power dissipation and temperature.

This paper presents an integrated readout circuit capable of measuring the power dissipated in a resistive transducer, as well as its temperature. It is designed for use with the CMOS-compatible tungsten-wire transducer reported in [19], but it has also been characterized in combination with a more robust commercial resistive micro-heater (Figaro TGS-8100 [20]) to evaluate the performance at power levels higher than what the CMOS-compatible transducers can handle. To obviate the need to stabilize or accurately measure the transducer's power dissipation, we adopt an alternative approach in which a second transducer acts as a thermal-conductivity reference. Its thermal properties are similar to those of the sensor, but it is shielded from the ambient air by appropriate packaging. Our readout circuit ratiometrically digitizes the sensor's thermal conductivity relative to that of the reference, without relying on accurate voltage, power or temperature references [21].

Measuring $CO_2$ variation through the change of the transducer's resistance is very challenging. Measurements of our tungsten-wire transducers show that a 200 ppm $CO_2$ variation causes a mere 0.3 mΩ variation in a baseline resistance of 110 Ω. The measurement can be relaxed by removing the baseline resistance, as only the change in resistance is of interest. Many approaches have been reported to cancel baseline resistance [22-25]. They either rely on a 'dummy' passive element but assume negligible mismatch errors introduced by manufacturing tolerances [22, 23], or require a dedicated calibration phase involving extra analog-to-digital conversion steps before measurements commence [24, 25].

To cancel the baseline resistance, this work adopts a two-state measurement. The transducers in our self-referenced system are operated alternately in 'hot' and 'cold' states by switching their bias-current levels, allowing the change in resistance between the two states to be measured directly. To not impose a challenging requirement on the dynamic range (DR) of the readout circuit due to the switching between 'hot' and 'cold' states, this work presents a novel structure employing pairs of dynamically-swapped transducers to cancel baseline resistance, thus enabling the accurate measurement of their resistance changes without increasing the DR requirement for the readout. In addition, dynamically-matched current sources are used to generate accurate current ratios for the 'hot' and 'cold' states, and the paired transducers are themselves periodically swapped to cancel errors due to transducer mismatch. Lastly, current-trimming DACs are used to further suppress mismatch errors.

Experimental results from a prototype implemented in a standard 0.16 μm CMOS process demonstrate the effectiveness of these techniques. In combination with the tungsten-wire transducers, the readout circuit achieves 14-bit resolution in the measured thermal resistance ratio, which corresponds to 228 ppm in $CO_2$ resolution (1σ) in a 70 s measurement time, while consuming 11.2 mW from a 1.8 V supply. An improved version of the design, in combination with the commercial micro-heaters, achieves 202 ppm $CO_2$ resolution in a measurement time of 30 s for the same power consumption.

The paper is organized as follows. In Section II, the operating principle of TC-based gas sensors and the proposed ratiometric readout circuit is presented. Section III is devoted to the circuit implementation of the readout circuit, including a switched-capacitor delta-sigma ADC,

dynamically-matched current sources, and current-trimming DACs. Experimental results and discussions are presented in Section IV, and the paper is concluded in Section V.

## II. OPERATING PRINCIPLE

### A. Thermal Resistance Measurement using a Resistive Transducer

A hot-wire transducer loses heat through two main paths, both of which can be modelled as thermal resistances, as shown in Fig. 1: one is to the surrounding air ($\theta_{air}$), the other is to the substrate via the anchor points ($\theta_{sub}$). The transducer's temperature rise relative to its ambient ($\Delta T$) caused by the power dissipated in the transducer ($P$) is directly proportional to the parallel combination $\theta$ of $\theta_{air}$ and $\theta_{sub}$:

$$\Delta T = P \times \theta = P \times (\theta_{air} \parallel \theta_{sub}) \quad (1)$$

Since the different components of air have different thermal conductivities, $\theta_{air}$ is a function of gas composition, and hence $\Delta T$ can be used to determine the $CO_2$ concentration in air. Since $CO_2$ is a better thermal insulator than air, higher $CO_2$ concentrations will lead to (slightly) higher values of $\Delta T$. To maximize sensitivity, heat loss to the substrate must be minimized. This is typically done by using suspended transducers [11, 18].

While $\Delta T$ in (1) can be measured using a dedicated temperature sensor (e.g., thermopiles [12]), the use of the electrical resistance of the heater to measure its temperature greatly simplifies the fabrication process, allowing the tungsten via material of a CMOS metal stack to be used as heater, as shown in Fig. 1a [19]. Tungsten is preferred over aluminium as the material of the resistive transducers for several reasons. First, in practice, aluminium is more difficult to process due to stiction in the wet release etch step. Second, the strength of the aluminium wire is worse

due to its grainy structure. Lastly, aluminium is more susceptible to electromigration.

The resistance of our tungsten transducers is in good approximation a linear function of temperature:

$$R = R_0 \cdot \left(1 + \alpha \cdot \left(T - T_0\right)\right) \tag{2}$$

where $R_0$ is the nominal electrical resistance of the transducer at room temperature $T_0$, and $\alpha$ its temperature coefficient. For our tungsten transducers, $R_0$ is 110 Ω and $\alpha$ is 0.0017/K. The nominal resistance $R_0$ is set by the aspect ratio of the resistor, and was designed to allow sufficient power to be dissipated in the resistor at the available voltage headroom.

To measure $\Delta T$, the transducer is alternately biased at a low current $I_c$ and a high current $I_h$ (Fig. 2a), corresponding to a 'cold' and a 'hot' state. The power dissipation in (1) then becomes the difference in power dissipation between these two states ($\Delta P$) , and $\theta$ becomes:

$$\theta = \frac{\Delta T}{\Delta P} = \frac{T_h - T_c}{P_h - P_c} = \frac{R_h - R_c}{R_0 \alpha \left(I_h^2 R_h - I_c^2 R_c\right)} \tag{3}$$

In order to accurately measure $\theta$, both $\Delta T$ and $\Delta P$ need to be accurately measured. The nominal $\theta$ of our tungsten transducer (at 400 ppm $CO_2$ and 25°C) is about 53,500 K/W. A change of 200 ppm $CO_2$ results in about 80 ppm change in the thermal resistance of air. For our transducers, the thermal resistance to the substrate ($\theta_{sub}$), which does not depend on the $CO_2$ concentration, is about two times larger than the thermal resistance to the surrounding air ($\theta_{air}$). Since the measured thermal resistance $\theta$ is the parallel combination of $\theta_{sub}$ and $\theta_{air}$, the relative sensitivity of $\theta$ to $CO_2$ is reduced by a factor 2/3 compared to that of $\theta_{air}$. Therefore, a $CO_2$ change of 200 ppm corresponds to a relative change of $\theta$ of about 50 ppm. This implies that the power levels

and temperature measurement should be stable to within ±25 ppm, making the measurement very challenging.

B. Ratiometric Thermal Resistance Measurement

Instead of measuring the absolute thermal resistance of one transducer, measuring the thermal resistance of a $CO_2$-sensitive transducer relative to that of a ($CO_2$-insensitive) reference transducer greatly relaxes the power stability and temperature measurement requirements, as the absolute accuracy requirement is replaced by a matching requirement of the $CO_2$-sensitive and reference transducers. The reference transducer is biased in the same way as the sensitive transducer (Fig. 2b). Their thermal-resistance ratio can be derived from (3) and expressed as a multiplication of two ratios: the ratio of the temperature-difference of the sensitive transducer ($\Delta T_s$) and the temperature-difference of the reference transducer ($\Delta T_r$), and the ratio of their power differences ($\Delta P_r$ / $\Delta P_s$):

$$\frac{\theta_s}{\theta_r}=\left(\frac{\Delta T_s}{\Delta T_r}\right)\left(\frac{\Delta P_r}{\Delta P_s}\right)=\left(\frac{R_{hs}-R_{cs}}{R_{hr}-R_{cr}}\right)\left(\frac{n^2I_c^2R_{hr}-I_c^2R_{cr}}{n^2I_c^2R_{hs}-I_c^2R_{cs}}\right)=\left(\frac{V_{hs}-nV_{cs}}{V_{hr}-nV_{cr}}\right)\left(\frac{nV_{hr}-V_{cr}}{nV_{hs}-V_{cs}}\right) \quad (4)$$

where $n = I_h / I_c$, $V_{hs} = n \cdot I_c \cdot R_{hs}$, $V_{cs} = I_c \cdot R_{cs}$, $V_{hr} = n \cdot I_c \cdot R_{hr}$, $V_{cr} = I_c \cdot R_{cr}$, and the transducers are assumed to have identical $R_0$ and $\alpha$, which therefore cancel out. The last term in (4) shows that the thermal-resistance ratio can be written as a product of two voltage-difference ratios, which in this work are digitized sequentially by a dual-mode switched-capacitor incremental ΔΣ ADC and multiplied in the digital backend.

Note that, while the ratiometric measurement relaxes the power and temperature measurement requirements, calibration and correction will still be needed due to device-to-device variation of the thermal resistance of the transducers and of their sensitivity. This

calibration will involve exposing the sensor to one or more well-defined $CO_2$ levels and measuring the ratiometric output. Also note that compensation for cross-sensitivity will be needed, since the transducers are also sensitive to e.g. temperature, humidity and pressure. This will involve co-integration of sensors for these parameters and correcting the output based on their readings. The implementation of this cross-sensitivity compensation is beyond the scope of this paper.

### C. Ratiometric Readout with Transducer Pairs

A challenge associated with the sequential readout of hot and cold states is that the voltage drop across the transducers varies significantly between the two states, which means that the following ADC must have a large dynamic range to avoid clipping. To relax the dynamic range, a pair of $CO_2$-sensitive transducers ($R_{s1}$, $R_{s2}$) and a pair of reference transducers ($R_{r1}$, $R_{r2}$) are used (Fig. 3). Both reference transducers are isolated from the ambient air by package-level sealing. In each pair, the transducers are alternately biased at $I_c$ and $I_h = n \cdot I_c$, generating simultaneously 'hot' and 'cold' voltages for both sensitive ($V_{hs}$, $V_{cs}$) and reference transducers ($V_{hr}$, $V_{cr}$). The current ratio $n$ is chosen so as to optimize the signal-to-noise ratio (SNR). For a given power consumed in biasing the transducers, a smaller $n$ gives a smaller signal amplitude, while a larger $n$ reduces the current in the 'cold' state, and, as a result, increases the noise level associated with that state. Therefore, SNR degrades for small and large values of $n$, and an optimum can be found for which the SNR is maximized. A parametric simulation of our design shows that this optimum is reached at a ratio of $n = 5$. The transducers in each pair are periodically swapped by the chopper switches around them, causing mismatches to be averaged out. To prevent the switching transients from affecting the measurement accuracy, a settling time is included after

swapping during which the ADC does not sample the voltages across the transducers. Since the thermal time constant of the transducers is relatively long (measured to be about 40 μs for our tungsten-wire transducers), the swapping is done at a relatively low rate (approximately once every 24 ms) to prevent the accumulated thermal settling time from significantly adding to the total measurement time. The 'hot' and 'cold' voltages are simultaneously sampled by scaled switched-capacitor circuits and merged together, as will be detailed in Section III.

## III. CIRCUIT IMPLEMENTATION

### A. Charge-Balancing Incremental ΔΣ Modulator

To obtain a $CO_2$-sensing resolution on the order of 200 ppm (corresponding to 50 ppm or 14.3 bits resolution in the $\theta$ ratio), we digitize each of the voltage ratios in (4) with a resolution better than 15.3 bits (equivalent to 100 ppm $CO_2$). Since $CO_2$ concentration tends to change relatively slowly, an incremental delta-sigma ADC is a suitable choice. A charge-balancing delta-sigma modulator is used that operates in two modes: temperature mode and power mode. First, in temperature mode, it produces a bitstream *bs* proportional to the first voltage ratio in (4), which equals the temperature-difference ratio. Then, in power mode, it produces a bitstream proportional to the second voltage ratio in (4), which equals the power-difference ratio. These bitstreams are decimated by an (off-chip) decimation filter, and the results are multiplied in the digital domain to obtain the thermal-resistance ratio.

Fig. 4 shows the switched-capacitor implementation of the modulator. It consists of a switched-capacitor integrator, with four parallel input branches connecting to the four transducers, and a

clocked comparator. To ensure accurate settling and to prevent integrator leakage from limiting the resolution, the integrator employs a gain-boosted folded-cascode OTA with a unity-gain bandwidth of about 2.5 MHz and a nominal DC gain of 140 dB [26]. The comparator is a latched comparator using a pre-amplifier to reduce kick-back effect of the positive-feedback latch [27]. Minimum-size switches (W/L = 0.8 μm/0.16 μm) are used to minimize charge injection.

To quantify the impact of various error sources from the circuit (e.g., the error in current ratio and the mismatch in capacitors) on the ADC's output, we designed a behavioral model for the transducer and the ADC based on a Verilog-A script and analyzed the sensitivities of the measured $\theta$ ratio to all the error sources. This analysis shows that accurate matching is required for the capacitors, and especially for the current sources in order to obtain accurate $CO_2$ measurements.

B. Switched-Capacitor Circuit in Temperature Mode

In temperature mode, the first voltage ratio in (4), which equals the temperature-difference ratio, is digitized. As shown in Fig. 4, the 'hot' voltages ($V_{hs}$, $V_{hr}$) are sampled by unit capacitors $C_s$ while the 'cold' voltages ($V_{cs}$, $V_{cr}$) are sampled by scaled capacitors $5C_s$, to generate the '$n$' factor in (4). The inaccuracy of this capacitor ratio gives an error in the measurement of the thermal-resistance ratio. Simulations show that 0.1% mismatch leads to a measurement error equivalent to 200 ppm $CO_2$. An accurate common-centroid layout is used to achieve this level of matching. Each transducer uses Kelvin connections to eliminate errors due to contact resistance. During phase $\varphi_1$, the 'hot' and 'cold' voltages are connected to one plate of the sampling capacitors,

while their other plate is connected to the common-mode voltage $V_{cm}$. During the subsequent phase $\varphi_2$, the connections to the transducers are reversed, while the capacitors are connected to the virtual ground of the integrator. This double-sampling scheme causes a charge proportional to two times the voltage drop across the transducer to be transferred to the integrator. The switches associated with the pair of sensitive transducers are gated by the bitstream, causing a charge proportional to $(V_{hs} - nV_{cs})$ to be integrated when $bs = 1$. Similarly, the switches associated with the reference transducers are gated by the inverse of the bitstream, causing a charge proportional to $-(V_{hr} - nV_{cr})$ to be integrated when $bs = 0$. Since the negative feedback in the modulator ensures that the average integrated charge tends to zero, the following charge-balancing equation applies:

$$\mu\left(V_{hs} - nV_{cs}\right) - (1-\mu)\left(V_{hr} - nV_{cr}\right) = 0 \quad \Rightarrow \quad \frac{1}{\mu} - 1 = \frac{V_{hs} - nV_{cs}}{V_{hr} - nV_{cr}} = \frac{R_{hs} - R_{cs}}{R_{hr} - R_{cr}} = \frac{\Delta T_s}{\Delta T_r} \qquad (5)$$

where $\mu$ is the fraction of ones in the bitstream, as determined by the decimation filter, which is a simple counter in this first-order modulator. This shows that the temperature-difference ratio can be readily derived from the decimated value.

The signal corresponding to $CO_2$ variations is extremely small. When the heating currents are 2.5 mA and 0.5 mA for the hot and cold states, respectively, the resulting resistance difference between the hot and cold states is about 5.8 Ω, while a 100 ppm increase in $CO_2$ concentration will only add 0.15 mΩ. This corresponds to the resistance resolution mentioned earlier of about 15.3 bits relative to the resistance difference (equivalent to about 19.5 bits relative to the total nominal resistance of 110 Ω).

To achieve this resolution, the noise in the system needs to be sufficiently small, including the

quantization noise of the ΔΣ ADC and the thermal noise contributed by the transducers, the bias currents, and the switched-capacitor circuit. These thermal noise sources manifest themselves as *kT/C* noise in the charge-balancing process, and can be reduced by increasing the unit-capacitor size $C_s$ or by increasing the over-sampling ratio (OSR) of the modulator [28]. At $C_s$ = 1 pF, chosen to limit the total die area, an over-sampling ratio (OSR) of at least $2^{18}$ is required . At this OSR, the modulator is limited by *kT*/*C* noise, since the quantization noise is well below the required level. The modulator is operated at a clock frequency of 83.3 kHz (one delta-sigma clock period is 12 μs), leading to a modulator-operating time of about 3.2 s. Including additional time for thermal settling of about 1.3 s, a total time of 4.5 s is needed to determine the temperature-difference ratio. This time can be reduced by increasing the capacitor sizes, or by increasing the clock frequency, both of which will translate into an increase in the power consumption of the modulator, but will help to reduce the energy consumed per measurement, because the overall power consumption is dominated by the transducers.

### C. Switched-Capacitor Circuit in Power Mode

In power mode, the voltage ratio proportional to the power-difference ratio in (4) is digitized. This is implemented by reconfiguring the switched-capacitor circuit with a reversed *bs* polarity (which is implemented, as shown in Fig. 4, by inverting *bs* after the quantizer). Moreover, the input voltages are connected through the cross-connections, so that the 'hot' voltages ($V_{hs}$, $V_{hr}$) are now sampled by the scaled capacitors $5C_s$, while the 'cold' voltages ($V_{cs}$, $V_{cr}$) are sampled by the unit capacitors $C_s$, thus realizing the '*n*' factor in the second voltage ratio of (4). Thus a charge proportional to ($nV_{hs} - V_{cs}$) from the sensitive transducers is continuously balanced by a charge proportional to $-(nV_{hr} - V_{cr})$ from the reference transducers, leading to a decimated output

μ that is a function of the second voltage ratio in (4), similar to the relation given in (5) for temperature mode. An important difference with temperature mode is that the signal charge that is processed is substantially larger, as is evident from (4). As a result, the OSR needed to reduce the thermal noise to the desired 15.3 bit level is much lower than the OSR needed in temperature mode. At this lower OSR, the first-order ΔΣ ADC becomes quantization-noise limited. Since the conversion during power mode takes only a fraction of the overall conversion time, a slightly higher OSR of $2^{16}$ is used than what is strictly required, to obtain a quantization-noise that meets the target with margin [29]. At a clock frequency of 83.3 kHz, this leads to a modulator-operating time of 0.8 s. Including additional time for thermal settling of about 0.7 s, a total time of 1.5 s is needed to determine the power-difference ratio. For a complete ratiometric thermal-resistance measurement, the modulator first spends 4.5 s in temperature mode and then 1.5 s in power mode, giving a total measurement time of 6 s.

### D. Dynamically-Matched Current Sources

Errors in the 1 : *n* bias current ratio lead to errors in the measured θ ratio. System-level simulations have shown that to reduce the resulting error in the measured $CO_2$ concentration to less than 200 ppm after a one-point offset trim, the current ratio should be accurate to 0.06%. To achieve this, dynamic element matching (DEM) is used (Fig. 5). Each transducer is associated with a set of 5 unit-current sources, each of which can be connected to the transducer via a switch. These switches are digitally controlled according to the DEM timing diagram shown in Fig. 5. When one sensitive transducer is biased by all five unit current sources (in the hot state), the other sensitive transducer is sequentially biased by one unit current source (in the cold state), generating an accurate average current ratio of five. The same biasing approach is applied to the

reference transducers. It should be noted that the current-domain chopping (indicated in Fig. 3) is also implemented by this switching scheme (switching between $I_c$ and $5I_c$). The reason for not physically swapping the two current outputs is that we include a current-trimming function to compensate for the mismatch of the transducers, as described in the next section.

### E. Current-Trimming DACs

In principle, the errors due to transducer mismatch are modulated to an AC signal by the periodic chopping of the transducers. However, it may still be necessary to trim the initial mismatch so that the ripple caused by the mismatch at the output of the first integrator will not overload the ΔΣ modulator. As shown in Fig. 6, the two currents $I_{OUT1}$ and $I_{OUT2}$, biasing the sensitive transducers $R_{s1}$ and $R_{s2}$ are generated using PMOS current mirrors (an identical circuit, not shown, is used for the reference transducers). A 6-bit binary-weighted current DAC (LSB current = 0.5% × $I_c$), embedded in the current source circuit, is used to trim the input current of these current mirrors, thus effectively compensating for the resistance mismatch between $R_{s1}$ and $R_{s2}$. Note that the current ratio between $I_{OUT1}$ and $I_{OUT2}$ does not need to be accurate, as long as both $I_{OUT1}$ and $I_{OUT2}$ provide an accurate 1 : $n$ current ratio sequentially to the individual transducers, which is ensured by the current-source DEM (Fig. 5). In this way, the measured thermal-resistance ratio is a ratio between the averaged thermal resistances of the two sensitive transducers and that of the two reference transducers.

## IV. EXPERIMENTAL RESULTS AND DISCUSSION

The readout circuit as well as the tungsten-wire transducers have been designed and fabricated in a 0.16 μm CMOS technology. Fig. 7 shows the layout plot and micrographs of the integrated

readout circuit and one of the transducers. The active die area of the circuit amounts to 0.7 $mm^2$, of which 0.37 $mm^2$ is occupied by the current sources and 0.33 $mm^2$ by the switched-capacitor $\Delta\Sigma$ modulator. The transducers are on another chip, fabricated using the same CMOS process followed by an etch step to release the wires, so as to be able to test different implementations of the transducers. To investigate the behavior at higher heating power levels, a commercial micro-heater was also used (Figaro TGS-8100, a metal-oxide-semiconductor gas sensor of which we use the integrated micro-heater) [20], which can withstand higher power and has similar electrical and thermal characteristics as the CMOS tungsten transducers. Four micro-heaters from four Figaro devices were connected to our readout circuits, two of which were sealed at the package to act as reference devices. For electrical measurements, the readout IC has been characterized in combination with this commercial micro-heater. Both the commercial heaters and the CMOS tungsten transducers have been used for $CO_2$ measurements.

A. Electrical measurements

Fig. 8 shows the measured current ratios of the dynamically-matched current sources for 4 samples of the readout IC. The initial mismatch of about ±0.2% is improved by an order of magnitude with DEM (better than the required 0.06% error budget). This proves that DEM effectively averages out the variations due to mismatch and thus improves the accuracy of thermal-resistance measurement.

Fig. 9 shows how the resolution of the thermal-resistance measurement (and hence the equivalent $CO_2$ resolution) varies as a function of the measurement time. Results of two versions of the circuit are shown. The first version employs a switched-capacitor circuit that samples the

transducer voltage on only one of the two clock phases [19]. The second version corresponds to the implementation discussed in Section III, employing the double-sampling scheme shown in Fig. 4. This scheme doubles the signal amplitude compared to the single-sampling scheme, while the noise level remains the same. Therefore, for the same measurement time, the SNR increases by 6 dB. The 2× improvement in $CO_2$ resolution observed in the experiment matches well with this expectation. At the targeted measurement time of 6 s, the second version of the readout circuit achieves an equivalent $CO_2$ resolution of 250 ppm (1σ) at ambient conditions in the lab. This is in reasonable agreement with the expectation based on a calculation of the input-referred signal-to-noise ratio as a function of OSR (dashed curve in Fig. 9). To achieve the targeted resolution of 200 ppm, a measurement time of 9 s is needed. For comparison, Fig. 9 also shows the measured $CO_2$ resolution at different controlled $CO_2$ levels (dashed curves and dash-dot curves), obtained from measurements performed in a climate chamber. These results will be discussed further in Section IV-B.

To demonstrate the insensitivity of the ratiometric measurement to the absolute current and power levels, Fig. 10 shows the measured temperature, power and thermal-resistance ratios as a function of $I_c$ (the bias current at the 'cold' state). For a ±10% change in $I_c$, the power ratio only changes by about ±10 ppm. For our $CO_2$ sensor, 200 ppm change in $CO_2$ will result in about 50 ppm change in thermal-resistance ratio, which requires the errors of power ratio to be within 25 ppm. Thus the measured results indicate that the ratiometric measurement effectively alleviates the dependence on the stability of the power dissipation. The measured thermal-resistance ratio also varies by about ±10 ppm, which could be due to the secondary temperature dependence of the thermal conductivity of air.

To demonstrate the effectiveness of the trimming scheme, Fig. 11 shows the measured temperature, power and thermal-resistance ratios, as well as the peak-to-peak voltage at the output of the integrator, for different current-trimming levels of the current sources that bias the sensitive transducers. The current trimming levels are indicated in LSB steps of the current DAC, where a negative number indicates the trimming current is added to one of the sensitive transducers ($R_{s1}$) and a positive number indicates the trimming current is added to the other sensitive transducer ($R_{s2}$). When the trimming level is less than 4 LSBs, the integrator's output swing is limited. For trimming levels above 8 LSBs, the integrator starts to clip, leading to large errors in the measured ratios. Note that in this particular case, the transducers are quite well matched, leading to an optimum for trimming level 0. In the case where transducers have larger mismatch, this current trimming function will suppress the initial mismatch between the transducers and thus prevent the modulator from clipping. Note that there is still some variation in the measured ratios when the trimming level is less than 4 LSBs. This is to be expected, since the trimming scheme always adds current to either of the two transducers and hence increases the power dissipation of the sensitive transducers. This will lead to a gain error in (4). In practice, such a gain error will be compensated for by the overall calibration of the sensor, along with the gain errors due to the tolerances on the nominal thermal resistances of the transducers.

To quantify the chip-to-chip variation introduced by the readout circuit, 18 samples of the chip have been measured in combination with the same set of off-chip fixed resistors. To exclude the effect of ambient variations, non-suspended resistors with a low temperature coefficient were used. To allow the circuit to operate with these resistors, the dynamic switching of the current

level was disabled, i.e. two resistors emulated a 'hot' resistance of about 120 Ω and two a 'cold' resistance of about 100 Ω. Since this mode of operation precludes the use of dynamic element matching, the measured spread includes the effect of current-source mismatch. In spite of this, the measured standard deviation of the decimated output is less than 0.6%. This is much less than the expected processing spread of the tungsten transducers, indicating that the spread due to the readout circuit is non-dominant and can be corrected for in the calibration procedure that will be needed for the transducers.

### B. $CO_2$ measurements

The first version of the readout circuit has been measured in combination with tungsten-wire transducers implemented in the back-end of a standard 0.16 µm CMOS process [19]. The sensitive and reference wires have a length of 250 µm. The cavity opening of the sensitive transducer is 200 µm, while that of the reference transducers is 50 µm. Both the approach of using a narrower etch window and the approach of package-level sealing to achieve a lower sensitivity of the thermal resistance to $CO_2$ in the reference device have been explored. Two transducer chips, each with a pair of transducers, were used. One chip, with the sensitive transducers, was packaged in a ceramic DIL package of which the cavity is exposed to the ambient air, and the other, with the reference transducers, was packaged in a DIL package of which the cavity is sealed. Note that there are potential solutions for sealing the reference transducers at the wafer-level, such as wafer-to-wafer capping, die-to-wafer bonding and wafer-level thin-film capping [30]. In this way, both types of transducers can in the future be integrated in the same package.

Fig. 12 shows the thermal-resistance ratio measured using the first version of the readout circuit while the $CO_2$ concentration was changed step-wise from 500 ppm to 9000 ppm. To reduce the noise level, which, as mentioned, is relatively high for the first version of the circuit, the measurement time was increased to 70 s for this experiment, at which the measured resolution is equivalent to 228 ppm $CO_2$ (1σ). The thermal-resistance ratio measured using the readout circuit has a sensitivity of 0.29 ppm/ppm $CO_2$, and shows good correlation with the $CO_2$ level measured using an NDIR-based reference sensor (Fig. 12a). Note that at the highest $CO_2$ level, this reference sensor was operated just beyond its full scale, causing its output to clip, but the parameters of the mass flow controllers that set the $CO_2$ concentration were correct.

As thermal-conductivity is not only sensitive to the change of $CO_2$, but is also highly influenced by environmental variations, we use reference temperature, humidity and pressure sensors to accurately measure the changes in ambient conditions, and determine the cross-sensitivities and then de-correlate the influences of these ambient variations by least-square curve fitting on the measurement results. The results after de-correlation are shown in Fig. 12b. These measurements were performed using a 2.5 mA bias current (hot state), at which the temperature rise of the tungsten transducer ($\Delta T$) is about 35°C above ambient temperature. When the bias current was increased to 5 mA ($\Delta T$ >100°C), a drifting behavior was observed.

The readout circuit has also been tested with discrete heaters: the micro-heaters in Figaro TGS-8100. The results are shown in Fig. 13, for both versions of the readout circuit. Four different $CO_2$ levels (500 ppm, 2500 ppm, 4500 ppm, 9000 ppm) and a baseline (pure air) were used in

this experiment. The thermal-resistance ratio measured has a sensitivity of 0.27 ppm/ppm $CO_2$, and shows good correlation with the reference $CO_2$ measurements.

In these experiments, a measurement time of 30 s was used, at which the second version of the readout circuit meets the targeted resolution of 200 ppm (Fig. 13b). As shown in Fig. 9, the $CO_2$ resolution measured at controlled $CO_2$ levels is about 370 ppm in a measurement time of 6 s, which is worse than the previous measurement at (uncontrolled) ambient conditions (250 ppm). This difference could be due to noise associated with airflow in the setup. As a result, a measurement time of 30 s is needed to meet the targeted resolution of 200 ppm. As expected, the resolution obtained with the first version of the circuit is approximately two times worse.

While the micro-heaters used can support higher power levels (the temperature rise at 2.5 mA bias current is about 20°C), only a very modest improvement in resolution was found when the power was increased. This is probably due to the fact that, while a higher power level gives a higher signal amplitude, it also reduces the sensitivity of the thermal conductivity of air to $CO_2$ concentration, due to the temperature dependency of this sensitivity.

A performance summary and comparison with other $CO_2$ sensors reported in literature as well as with a commercial product is shown in Table I. Compared with other TC-based $CO_2$ sensors, the $CO_2$ transducer (tungsten wire) and readout circuit in this work are both implemented in standard CMOS technology with minimum post-processing steps, unlike the special MEMS processes required to fabricate the other transducers. The active die area of the sensor including readout circuit is about 3 $mm^2$ which is much smaller than that of the sensor in [12] or [13]. The first

version of the chip in combination with the CMOS tungsten-wire transducers achieves 228 ppm $CO_2$ resolution in 70 s in the indoor $CO_2$ range (at 500 ppm level), which is 2× better than the resolution reported in [13]. In combination with the commercial heaters (Figaro TGS-8100), the same readout achieves 400 ppm resolution in 30 s. The second version of the chip (with double sampling) in combination with commercial heaters (Figaro TGS-8100) achieves 202 ppm resolution in 30 s. As most of the power is used for heating the transducer, reducing the power consumption of readout circuit would only lead to a minor improvement. To optimize the design for energy efficiency, further improvement can be made in decreasing the measurement time, which can be done by increasing the size of the switches and operating the modulator at a clock frequency. Alternatively, the capacitor size can be further increased to reduce the circuit noise, at the cost of increased die size. Note that in the latter case, the size of switches should also be increased in order to meet the settling requirement of the switched-capacitor circuit.

## V. CONCLUSIONS

In this work, we have reported a novel readout circuit for ratiometric thermal-conductivity measurement. The circuit digitizes both the temperature rise and the power dissipation of $CO_2$-sensitive transducers relative to that of reference transducers, from which their thermal-resistance ratio can be calculated, thus circumventing an accurate power reference. Experimental results have shown that for a ±10% change in bias current, the measured power ratio between sensitive and reference transducers only changes by about ±10 ppm. A pair of gas-sensitive transducers is combined with a pair of reference transducers to cancel baseline resistance, thus greatly relaxing the dynamic range requirement of the ADC. The transducers are dynamically swapped during a conversion to dynamically cancel out the errors due to transducer mismatch. An accurate current

ratio between 'hot' and 'cold' states is generated by dynamically-matched current sources, and furthermore, a 6-bit current DAC is used to trim the transducers to ensure that the residual mismatch will not overload the ΔΣ modulator. Experimental results show that the applied techniques are effective, and using this ratiometric readout circuit, a CMOS-compatible thermal-conductivity-based $CO_2$ sensor achieves 228 ppm (1σ) $CO_2$ resolution. To further evaluate the capability of the readout circuit, we use micro-heaters in Figaro TGS 8100 as a substitute for tungsten-wire transducers. The second version of the design achieves 200 ppm resolution over a $CO_2$ range of 500 to 9000 ppm, which indicates that high-resolution TC-based $CO_2$ sensing is attainable even with on-chip electronics, thus facilitating the realization of fully-integrated $CO_2$ sensors for air-quality monitoring, which are much smaller and less expensive than current $CO_2$ sensors.

## ACKNOWLEDGMENT

This work is supported by NXP Semiconductors and austriamicrosystems AG (AMS). The authors want to thank Zu-yao Chang and Lukasz Pakula for their technical support.

## REFERENCES

[1] "Gas Sensors Market - Global Industry Size, Share, Trends, Analysis and Forecast 2012 – 2018", Transparency Market Research [Online]. Available: http://www.transparencymarketresearch.com/gas-sensors-market.html.

[2] U. Satish, et al., "Is $CO_2$ an indoor pollutant? direct effects of low to moderate $CO_2$ concentrations on human decision-making performance," Environmental health perspectives, 2014.

[3] S.J. Emmerich, A.K. Persily, "Literature review on $CO_2$-based demand-controlled ventilation," ASHRAE Transaction, vol. 103, pp. 229–243, 1997.

[4] K. Kaneyasu, et al., "A carbon dioxide gas sensor based on solid electrolyte for air quality control," Sens. Actuators B: Chem., vol. 66, pp. 56-58, Jul. 2000.

[5] S. Yi, et al., "Novel NDIR $CO_2$ sensor for indoor air quality monitoring," in Proc. IEEE Int. Conf. on Solid-State Sensors, Actuators and Microsystems (Transducers '05), 2005, pp. 1211-1214.

[6] K. Souri, Y. Chae and K.A.A. Makinwa, "A CMOS Temperature Sensor With a Voltage-Calibrated Inaccuracy of ±0.15°C (3σ) From -55 °C to 125 °C", IEEE J. Solid-State Circuits, vol. 48, no. 1, pp. 292-301, Jan. 2013.

[7] M. A. P. Pertijs, K. A. A. Makinwa, and J. H. Huijsing, "A CMOS smart temperature sensor with a 3σ inaccuracy of ±0.1 °C from -55 °C to 125 °C," IEEE J. Solid-State Circuits, vol. 40, no. 12, pp. 2805-2815, Dec. 2005.

[8] Z. Tan, et al., "A 1.2-V 8.3-nJ CMOS humidity sensor for RFID applications," IEEE J. Solid-State Circuits, vol. 48, no. 10, pp. 2469-2477, Oct. 2013.

[9] SenseAir K30 datasheet, SenseAir [Online]. Available: http://www.senseair.com/.

[10] G. U. Gamm, et al., "Low power wireless sensor node for use in building automation," in Proc. 12th IEEE Wireless and Microwave Technology Conference (WAMICON), 2011, pp. 1-6.

[11] I. Simon and M. Arndt, "Thermal and gas-sensing properties of a micromachined thermal conductivity sensor for the detection of hydrogen in automotive applications," Sens. Actuators A: Phys., vol. 97–98, pp. 104-108, Apr. 2002.

[12] K. Kliche, et al., "Sensor for gas analysis based on thermal conductivity, specific heat capacity and thermal diffusivity," in Proc. IEEE Int. Conf. on MEMS, 2011, pp. 1189-1192.

[13] K. Kliche, et al., "Sensor for thermal gas analysis based on micromachined silicon-microwires," IEEE Sensors J., vol. 13, pp. 2626-2635, Jul. 2013.

[14] N. Tadic, M. Zogovic, and D. Gobovic, "A CMOS controllable constant-power source for variable resistive loads using resistive mirror with large load resistance dynamic range," IEEE Sensors J., vol. 14, pp. 1988-1996, Jun. 2014.

[15] S. Chan and P. C. Chan, “A resistance-variation-tolerant constant-power heating circuit for integrated sensor applications,” IEEE J. Solid-State Circuits, vol. 34, no. 4, pp. 432–439, Apr. 1999.

[16] C.A. Leme, R. Lenggenhager, I. Filanovsky, H. Baltes, "Linear CMOS power controller for precision sensor applications," in Proc. IEEE Int. Symp. Circuits Syst., 1992, pp. 1844-1846.

[17] S. Sarfraz, R. V. Kumar, and F. Udrea, "A high temperature and low power SOI CMOS MEMS based thermal conductivity gas sensor," in Proc. IEEE Int. Semiconductor Conf., 2013, pp. 51-54.

[18] S. Z. Ali, et al., "Tungsten-based SOI microhotplates for smart gas sensors," J. Microelectromech. Syst., vol. 17, pp. 1408-1417, Dec. 2008.

[19] Z. Cai, et al., "An integrated carbon dioxide sensor based on ratiometric thermal-conductivity measurement," in Proc. IEEE Int. Conf. on Solid-State Sensors, Actuators and Microsystems (Transducers '15), 2015, pp. 622-625.

[20] FIGARO TGS8100 datasheet (rev06), FIGARO [Online]. Available: http://www.figaro.co.jp/.

[21] Z. Cai, et al., "A ratiometric readout circuit for thermal-conductivity-based resistive gas sensors," in Proc. ESSCIRC, 2015, pp. 275-278.

[22] N.M. Mohan, B. George and V.J. Kumar, "A novel dual-slope resistance-to-digital

converter," IEEE Trans. Instrum. Meas., vol. 59, no. 5, pp. 1013-1018, May 2010.

[23] C. K. Leung and D. M. Wilson, "Integrated interface circuits for chemiresistor arrays," in Proc. IEEE Int. Symp. Circuits Syst., 2005, pp. 5914-5917.

[24] X. Mu, et al., "CMOS monolithic nanoparticle-coated chemiresistor array for micro-scale gas chromatography," IEEE Sensors J., vol. 12, no. 7, pp. 2444-2452, Jul. 2012.

[25] M. Grassi, P. Malcovati, and A. Baschirotto, "A 160 dB equivalent dynamic range auto-scaling interface for resistive gas sensors arrays," IEEE J. Solid-State Circuits, vol. 42, no. 3, pp. 518-528, Mar. 2007.

[26] K. Bult and G. J. G. M. Geelen, "A fast-settling CMOS op amp for SC circuits with 90-dB DC gain," IEEE J. Solid-State Circuits, vol. 25, no. 6, pp. 1379-1384, Dec 1990.

[27] H. Fiedler, et al., “A 5-bit building block for 20 MHz A/D converters,” IEEE J. Solid-State Circuits, vol. 16, no. 3, pp. 151–155, Jun. 1981.

[28] R. Schreier, J. Silva, J. Steensgaard and G. C. Temes, "Design-oriented estimation of thermal noise in switched-capacitor circuits," IEEE Trans. Circuits Syst., I, Regular papers, vol. 52, no. 11, pp. 2358-2368, Nov. 2005.

[29] J. Markus, J. Silva, and G. C. Temes, “Theory and applications of incremental ΔΣ converters,” IEEE Trans. Circuits Syst. I, Fundam. Theory Applicat., vol. 51, no. 4, pp. 678–690, Apr. 2004.

[30] K. Seetharaman, et al., "A robust thin-film wafer-level packaging approach for MEMS devices." J. Microelectronics and Electronic Packaging, vol. 7, pp. 175-180, Jul. 2010.

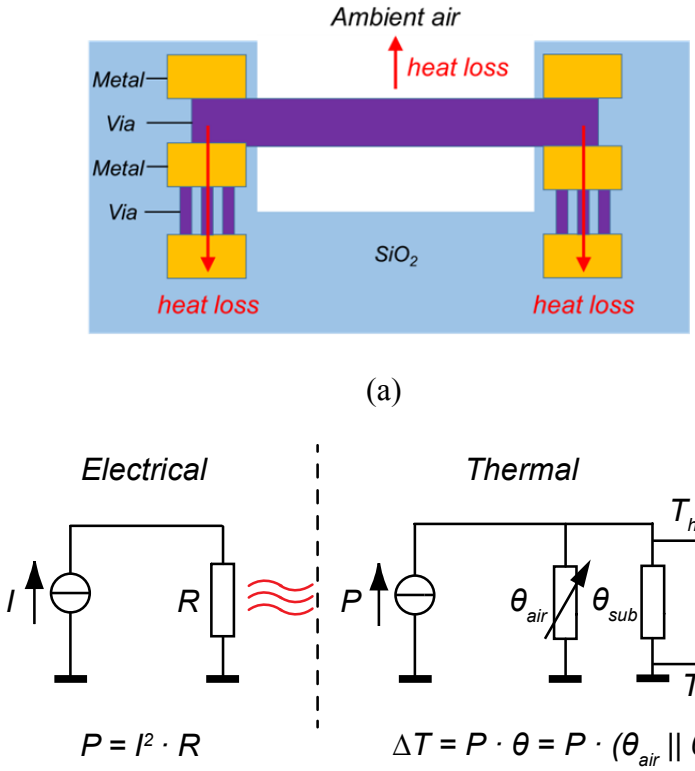


Fig. 1. Steady-state thermal resistance measurement principle; (a) cross-sectional view of a suspended hot-wire resistive transducer and its heat-loss paths and (b) the equivalent model in both electrical and thermal domains

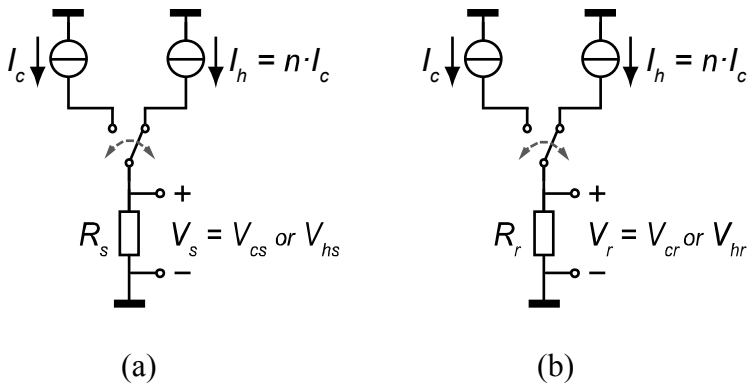


Fig. 2. (a) $CO_2$-sensitive and (b) reference transducer alternately biased at two different current levels

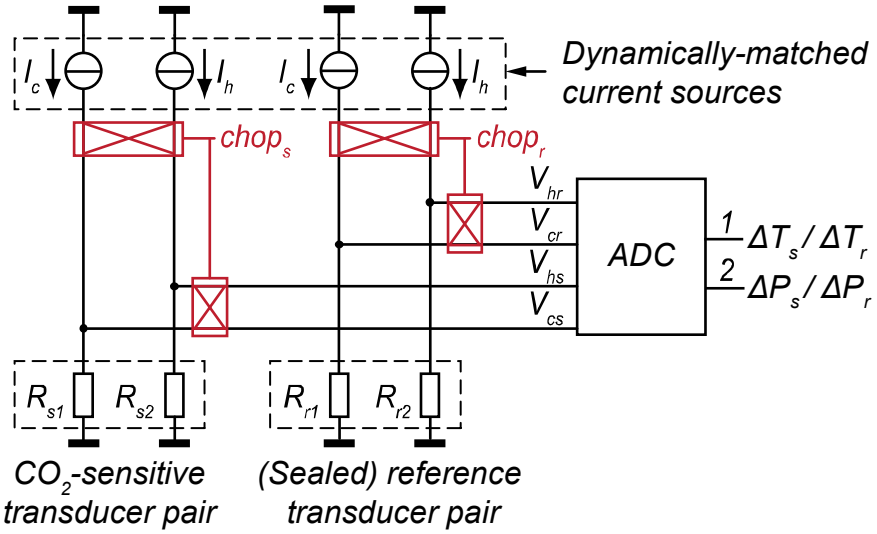


Fig. 3. Block diagram of the ratiometric thermal-conductivity sensor readout with transducer pairs for baseline-resistance cancellation

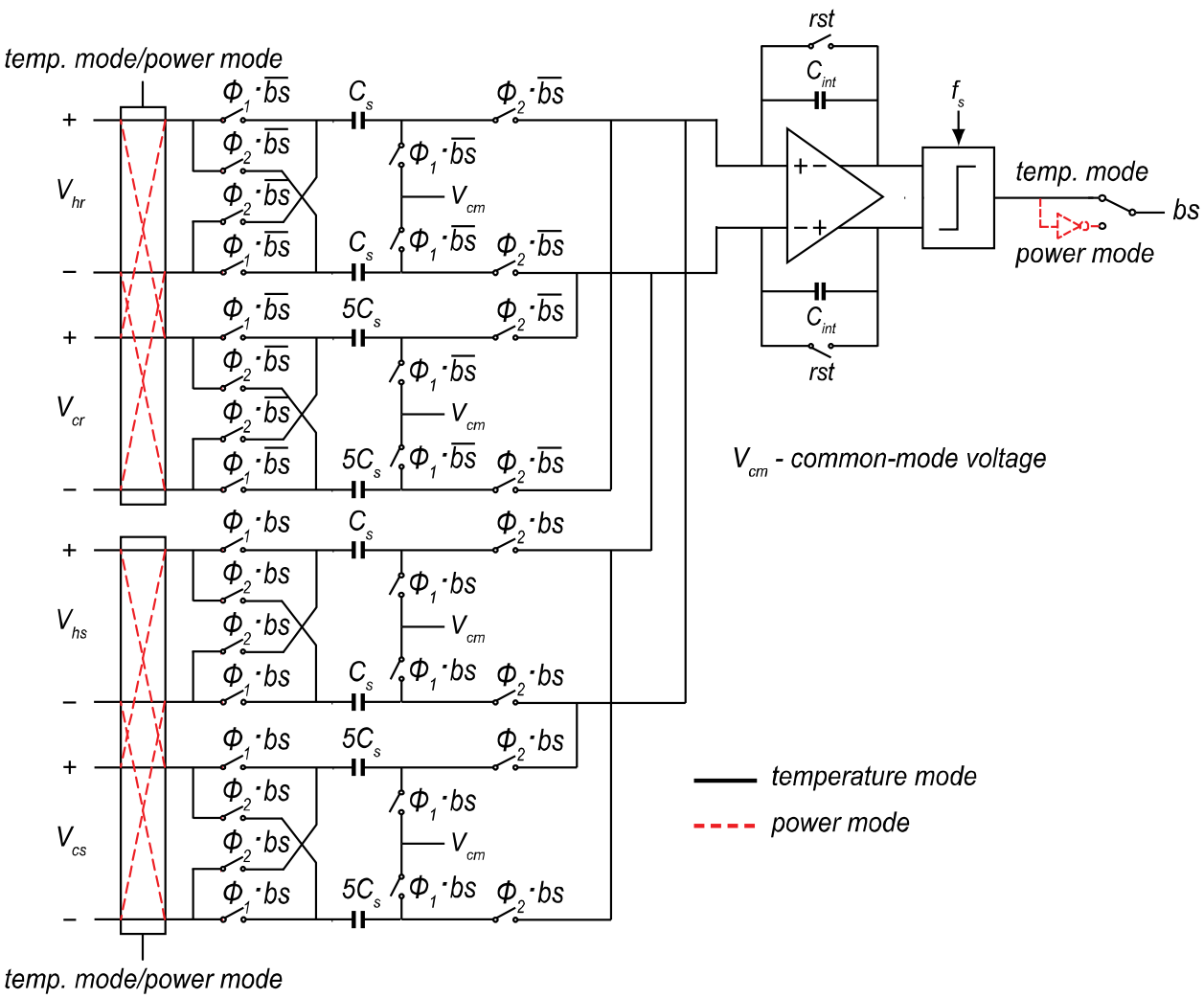


Fig. 4. Simplified circuit diagram of the switched-capacitor delta-sigma modulator in both temperature and power modes

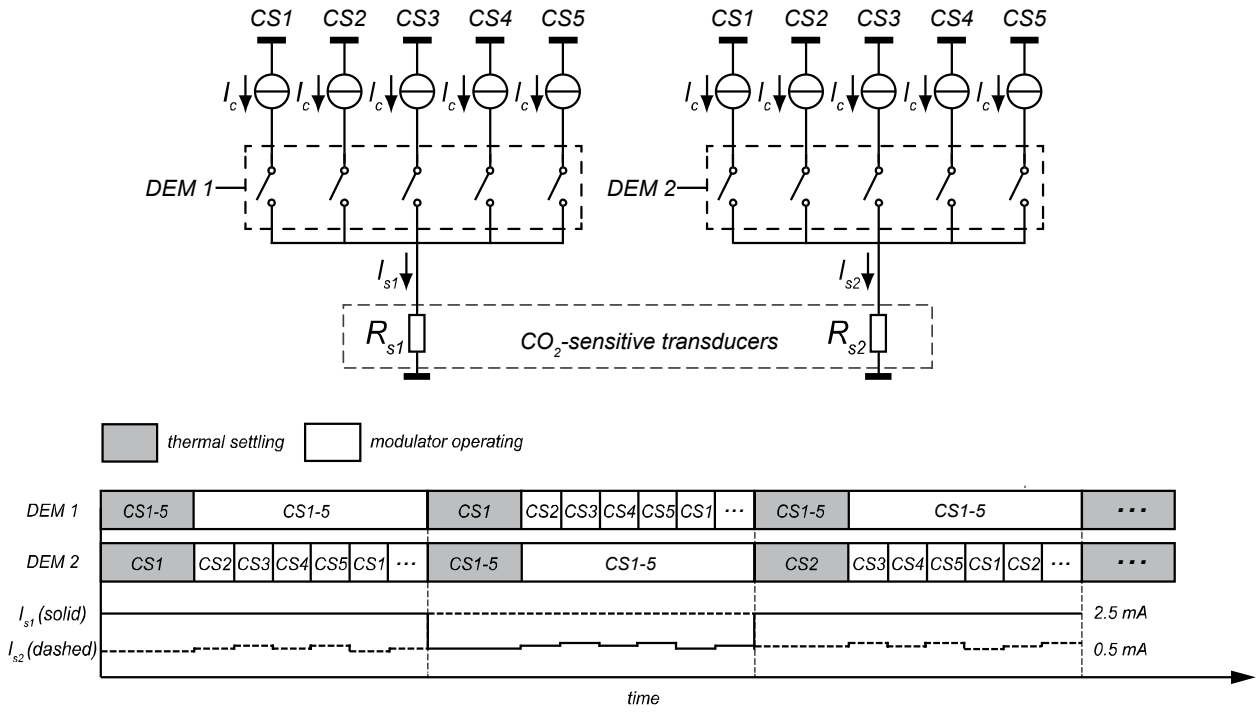


Fig. 5. Dynamically-matched current sources and associated timing diagram (same algorithm applies to the current sources for the reference transducers)

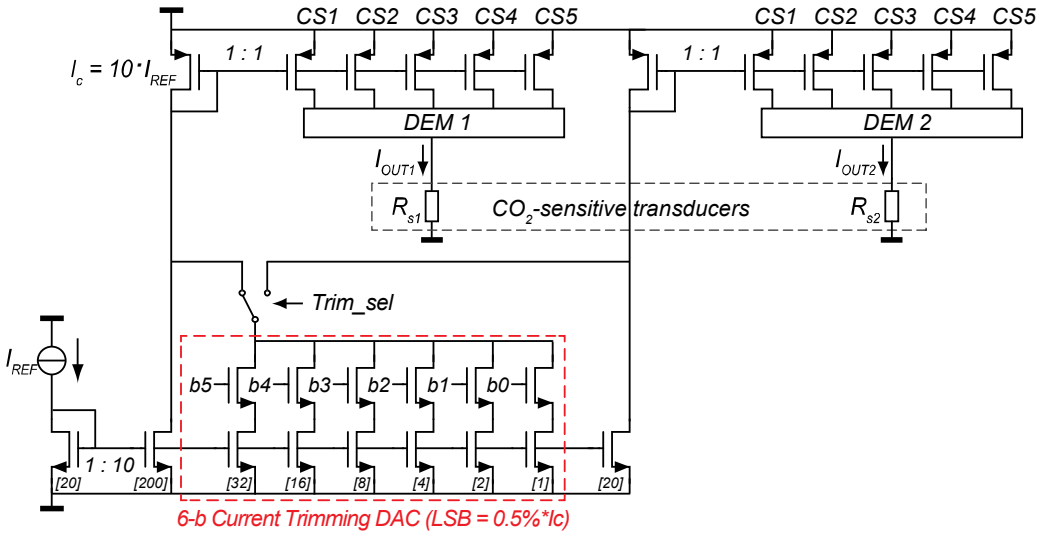


Fig. 6. Circuit diagram of the current sources with a 6-bit current trimming DAC (LSB current = 0.5% × $I_c$; the current sources as well as the current trimming DAC for the reference transducers are identical, not shown here; cascode transistors omitted for simplicity)

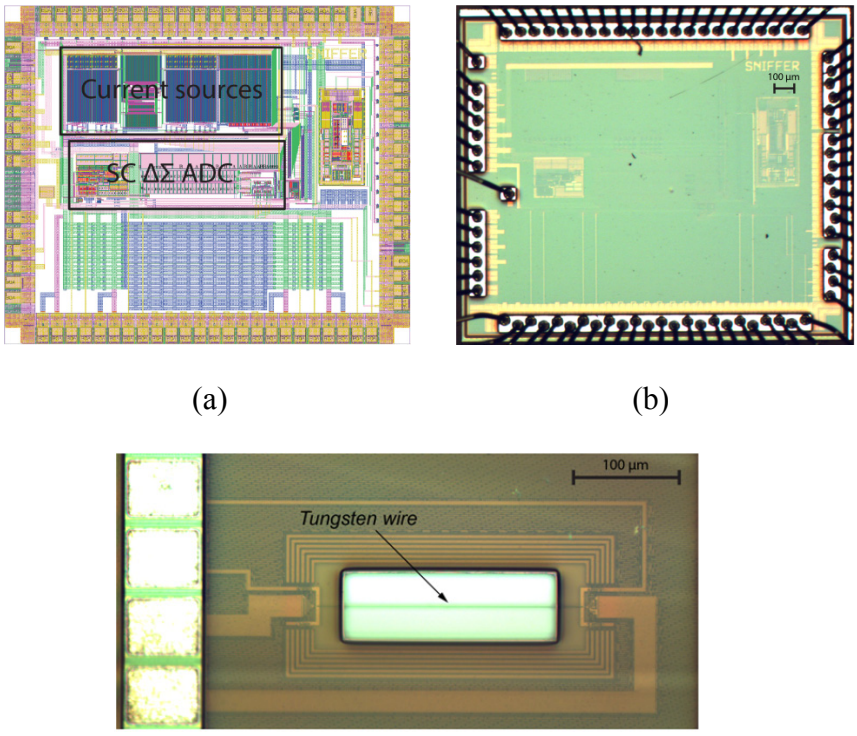


Fig. 7. (a) Layout plot, (b) micrograph of the integrated readout circuit and (c) micrograph of a CMOS-compatible tungsten-wire transducer (using Kelvin connections, two wide tracks for current driving and two narrow tracks for voltage sensing)

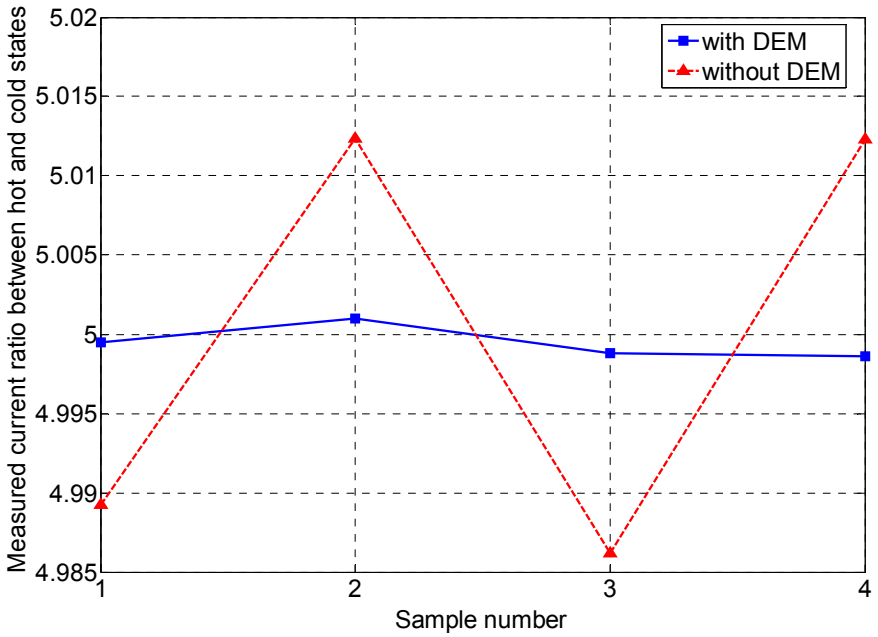


Fig. 8. Measured current ratios of the dynamically-matched current sources on 4 samples of the chip (initial mismatch is about 0.2%; after DEM the inaccuracies are -0.01%, 0.02%, -0.02% and -0.03% respectively)

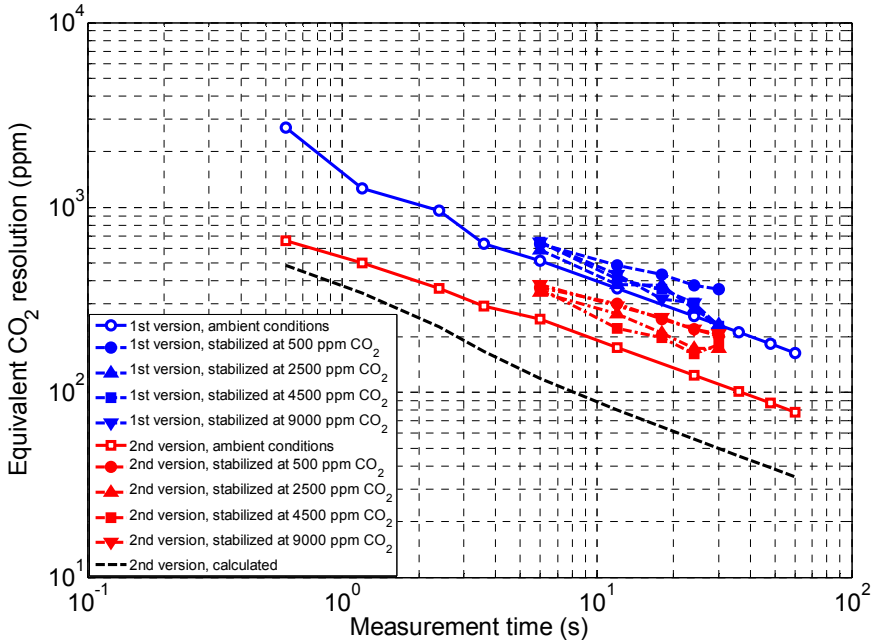

Fig. 9. Equivalent $CO_2$ resolution (1σ) derived from the standard deviation of the measured thermal-resistance ratio at ambient conditions (solid curves) and at different controlled $CO_2$ levels, using the first version (single-sampling) and the second version (double-sampling) of the readout circuit in combination with Figaro micro-heaters, along with the calculated resolution of the double-sampling scheme.

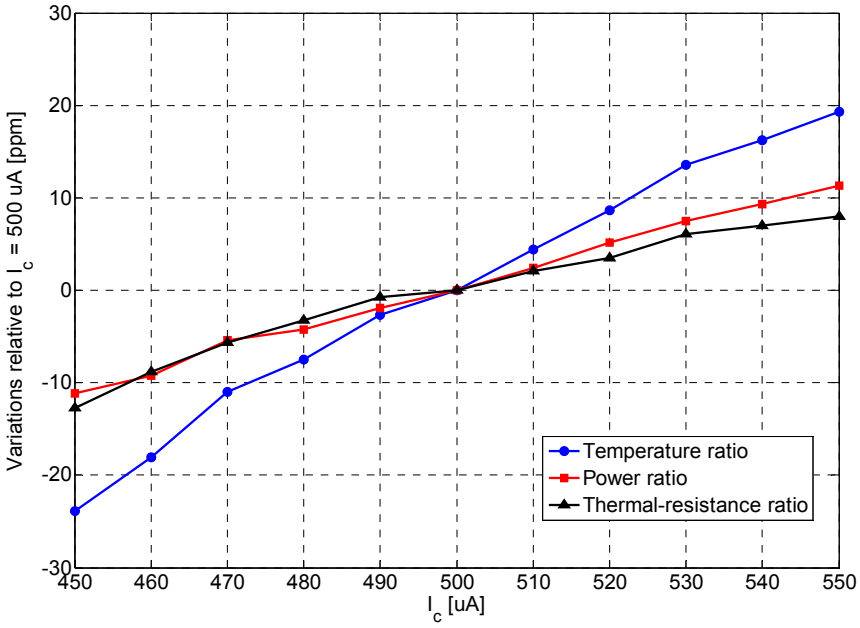


Fig. 10. Variations in temperature, power and thermal-resistance ratios between the sensitive and reference transducers as a function of the bias current at 'cold' state ($I_c$)

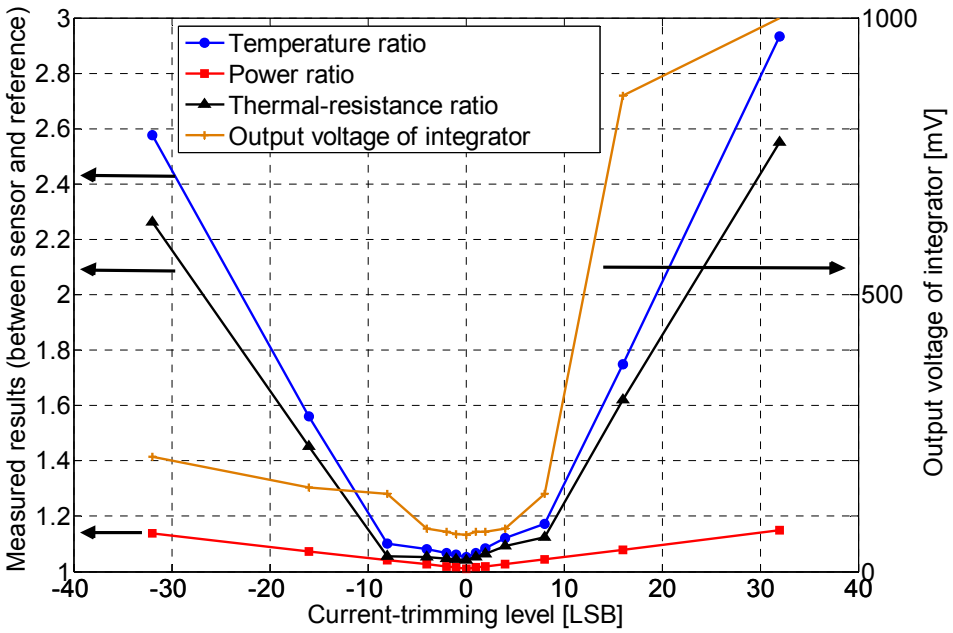


Fig. 11. Temperature, power, thermal-resistance ratios and the (peak-peak) voltage at the output of the integrator as a function of the current trimming level (in LSB steps of the trimming DAC)

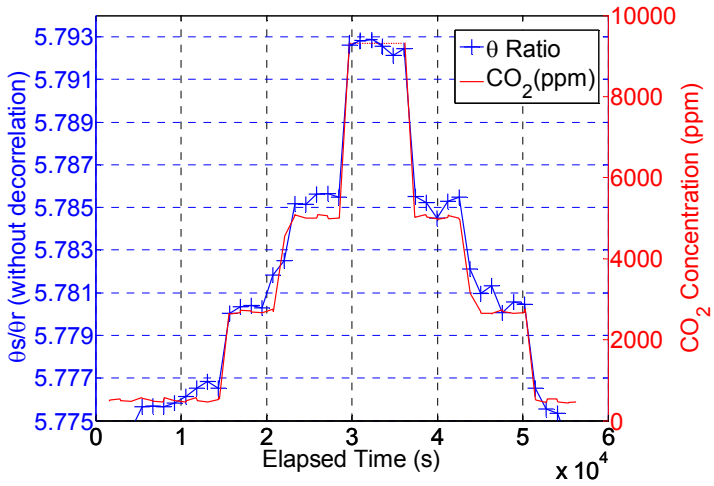


(a)

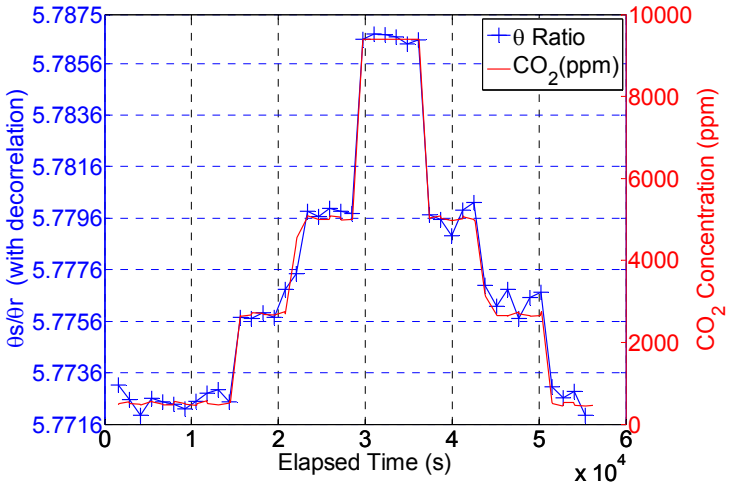


(b)

Fig. 12. Thermal-resistance ratio measured using the first version of the readout circuit with a 70 s measurement time, in combination with tungsten-wire transducers, for step-wise changing $CO_2$ concentration, without (a) and with (b) compensation for temperature and pressure cross-sensitivity, along with $CO_2$ concentration measured using an accurate reference NDIR sensor.

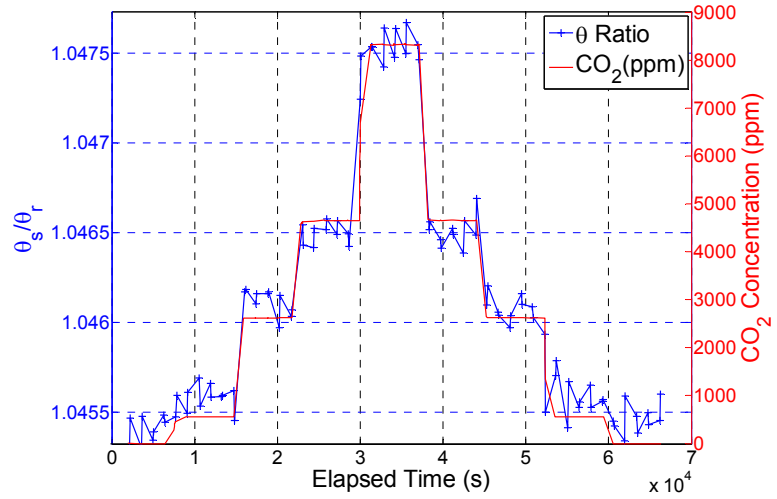


(a)

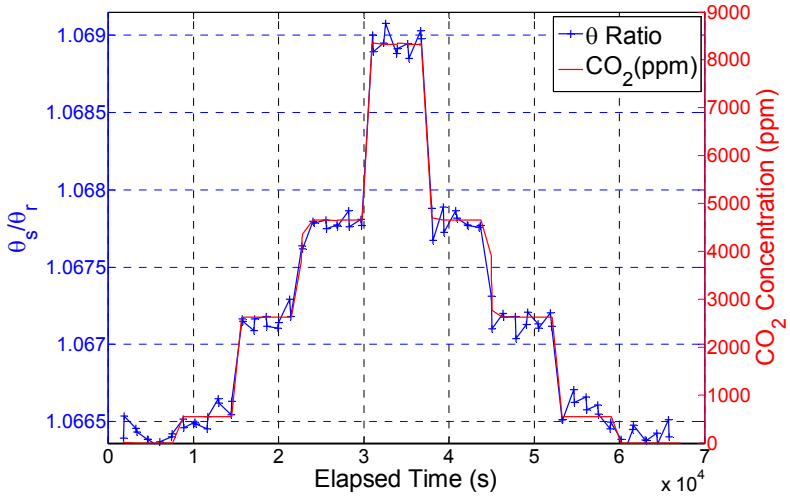


(b)

Fig. 13. Thermal-resistance ratio measured using the first (a) and second (b) version of the readout circuit, both with a 30 s measurement time, in combination with Figaro TGS 8100 transducers, with compensation for temperature and pressure cross-sensitivity, for step-wise changing $CO_2$ concentration, along with $CO_2$ concentration measured using an accurate reference NDIR sensor.

TABLE I: Performance of the proposed sensor compared to the prior art

| Parameter | This work | | | [13] | [12] | IR11BD |
|---|---|---|---|---|---|---|
| Method | TC | | | TC | TC | NDIR |
| Technology | CMOS | | | SOI MEMS | SOI MEMS | – |
| Readout IC | Yes | | | No | No | No |
| Die size | 3 $mm^2$ | | | 16 $mm^2$ | 9 $mm^2$ | – |
| Supply voltage | 1.8 V | | | – | – | 3-15 V |
| Power (sensor) | 10.8 mW | | | 3 mW | 7 mW | 180 mW |
| Power (readout) | 0.4 mW | | | – | – | – |
| | 1st version | 1st version | 2nd version | | | |
| Meas. time | 70 s | 30 s | 30 s | 60s | N/A | 20s |
| $CO_2$ resolution (1σ) | 228 ppm* | 400 ppm† | 202 ppm† | 456 ppm | <1% | <100 ppm |

* In combination with CMOS-compatible tungsten-wire transducers

† In combination with discrete micro-heaters (Figaro TGS 8100) [20]